Atmos. Chem. Phys. Discuss., 12, 18379–18418, 2012
www.atmos-chem-phys-discuss.net/12/18379/2012/
doi:10.5194/acpd-12-18379-2012

Atmospheric Chemistry and Physics Discussions

The Arctic response to remote and local forcing of black carbon

M. Sand[1], T. K. Berntsen[1], J. E. Kay[2], J. F. Lamarque[2], Ø. Seland[3], and A. Kirkevåg[3]

[1]Department of Geosciences, Meteorology and Oceanography Section, University of Oslo, Oslo, Norway
[2]National Center for Atmospheric Research, Boulder, Colorado, USA
[3]Norwegian Meteorological Institute, Oslo, Norway

Received: 15 June 2012 – Accepted: 4 July 2012 – Published: 26 July 2012

Correspondence to: M. Sand (maria.sand@geo.uio.no)

Published by Copernicus Publications on behalf of the European Geosciences Union.

Abstract

Recent studies suggest that the Arctic temperature response to black carbon (BC) forcing depend on the location of the forcing. We investigate how BC in the mid-latitudes remotely influence the Arctic climate, and compare this with the response to BC located in the Arctic it self. In this study, idealized climate simulations are carried out with a fully coupled Earth System Model, which includes a comprehensive treatment of aerosol microphysics. In order to determine how BC transported to the Arctic and BC sources not reaching the Arctic impact the Arctic climate, forcing from BC aerosols is artificially increased by a factor of 10 in different latitude bands in the mid-latitudes (28°N–60°N) and in the Arctic (60°N–90°N), respectively. Estimates of the impact on the Arctic energy budget are represented by analyzing radiation fluxes at the top of the atmosphere, at the surface and at the lateral boundaries. Our calculations show that increased BC forcing in the Arctic atmosphere reduces the surface air temperature in the Arctic with a corresponding increase in the sea-ice fraction, despite the increased planetary absorption of sunlight. The analysis indicates that this effect may be due to a combination of a weakening of the northward heat transport caused by a reduction in the meridional temperature gradient and a reduction in the turbulent mixing of heat downward to the surface. The latter factor is explained by the fact that most of the BC is located in the free troposphere and causes a warming at higher altitudes which increases the static stability in the Arctic. On the other hand we find that BC forcing at the mid-latitudes warms the Arctic surface significantly and decreases the sea-ice fraction. Our model calculations indicate that atmospheric BC forcing outside the Arctic is more important for the Arctic climate change than the forcing in the Arctic itself. Although the albedo effect of BC on snow does show a more regional response to an Arctic forcing, these results suggest that mitigation strategies for the Arctic climate should also address BC sources in locations outside the Arctic even if they do not contribute much to BC in the Arctic.

ACPD

12, 18379–18418, 2012

1 Introduction

Arctic temperatures have increased at a rate about twice as fast as the global mean rate during the last decades (AMAP, 2011). Many inter-related factors arising both from internal climate variability and external climate forcing could have contributed to this greater-than-global Arctic warming. These factors include local feedbacks (snow/ice-albedo, clouds), increased poleward heat transport, and enhanced forcing by absorbing aerosols (black carbon) (IPCC, 2007). Accompanied by the temperature increase, the Arctic has experienced a longer melt season with an earlier spring melt and a decrease in the sea-ice extent (AMAP, 2011). Black carbon (BC) aerosols absorb solar radiation and heat the surrounding air. This direct effect of BC may be potentially large in the Arctic, as the absorbing aerosols are located over highly reflective snow/ice surfaces (Pueschel and Kinne, 1995; Hansen and Nazarenko, 2004). In general added atmospheric heat will increase the downward fluxes of longwave radiation and sensible heat, and thus warm the underlying surface. However, models and measurements (Koch et al., 2009) indicate that BC aerosols are located mainly in the free troposphere and in may further stabilize the Arctic atmosphere, thereby limiting the downward flux of sensible heat and the potential surface warming.

BC aerosols in the Arctic originate from emissions mainly at mid-latitudes that are transported northwards (Barrie, 1986; Law and Stohl, 2007). Sources of BC include both anthropogenic sources (e.g. energy and industrial production, domestic combustion and transport) and natural sources (forest and grassfires induced from lightening). During winter the northward transport is strongest, and the lifetime of BC in the atmosphere is longer, causing a maximum BC concentration in the Arctic in late winter and spring (Sharma et al., 2006). The elevated BC concentrations also extend into the melting season, which could make BC particularly important in the Arctic. BC aerosols affect the atmospheric temperature gradients and can therefore change the atmospheric heat transport and the distribution of clouds. In addition, BC aerosols can have an indirect effect on clouds by acting as cloud condensation nuclei or ice nuclei and influence

ACPD
12, 18379–18418, 2012

the cloud cover and cloud lifetime via microphysical interactions. BC can also affect the distribution of clouds by changing the stability of the atmosphere, often referred to as the semi-direct effect (Koch and Genio, 2010).

BC affects the climate in numerous ways and there are large uncertainties in estimating the net BC forcing. Because of the short lifetime of BC compared to well-mixed greenhouse gases, BC has a potential for short-term climate control strategies (Hansen et al., 2000; Levy et al., 2008; Jacobson 2010; Shindell et al., 2012). In order to identify the best options for emission reductions there is a need for improving the understanding of the role of BC aerosols in the Arctic (AMAP, 2011) and how the response of the Arctic climate depends on the location of BC forcing. Shindell (2007) demonstrated that the climate response in the Arctic is highly correlated with mid-latitude forcing during non-summer seasons, due to the large-scale dynamics influencing the Arctic climate. In these months the Arctic surface temperature response can show opposite signs to the local forcing. Results from Menon et al. (2002) also indicate that forcing from BC can have a climate impact away from the forcing area, by local atmospheric heating and dynamical transport. Shindell and Faluvegi (2009) perturbed forcings by enhancing the concentrations of BC aerosols in different latitude bands and found that for the Arctic latitude band, the Arctic surface air temperature (SAT) decreased, despite a positive forcing at the top of the atmosphere. Shindell and Faluvegi attributed this to a reduction in the pole-ward heat flux following increased absorption of incoming solar radiation by BC and strong local heating in the free troposphere. For positive direct forcing by BC aerosols in the mid-latitude band the Arctic surface temperature response was positive (warming).

The results from the study of Shindell and Faluvegi (2009) were somewhat unexpected, and with the increasing focus on the effect of BC aerosols on the Arctic climate, there is a need to verify that the results are robust by reproducing parts of the experiment with a different climate model; to analyze the Arctic climate response to BC perturbations in the Arctic (60° N–90° N) and northern mid-latitude (28° N–60° N) atmosphere, respectively. To extend the study a bit further, we want to understand and

ACPD
12, 18379–18418, 2012

quantify the contribution from the different processes that are important for BC forcing and response in the Arctic, including a comprehensive study of the Arctic heat budget. Idealized climate simulations with artificially increased BC concentrations in the two separate latitude bands have been performed with a fully coupled earth system model, the NorESM, to include feedbacks from sea ice cover and sea surface temperatures (SST's). The atmospheric model includes a comprehensive treatment of aerosol microphysics, accounting for aerosol nucleation, condensation, coagulation and cloud processing, and calculates the conversion of BC to a hydrophilic state where it can be scavenged by precipitation. The wet deposition is calculated in full integration with the cloud and precipitation schemes. The two experiments are compared with a control run to analyze the response in the Arctic temperatures to the two forcings, including changes in feedbacks from sea-ice, cloud cover and the meridional energy transport into the Arctic.

2 Data and methods

2.1 NorESM

The climate model used in this study is the Norwegian Earth System Model, NorESM (Kirkevåg et al., 2008, 2012; Seland et al., 2008), to a large extent based on the Community Climate System Model CCSM4.0 (Gent et al., 2011), developed at the National Center for Atmospheric Research (NCAR). The model is run fully coupled with an atmospheric model, an ocean model, a land model, and a sea-ice model. The atmospheric part of NorESM, CAM4-Oslo, has applied aerosol and cloud droplet parameterization schemes developed for CAM-Oslo based on CAM3, which is a further elaborated version of a previous aerosol module (Iversen and Seland, 2002, 2003; Kristjánsson, 2002). The ocean model in NorESM, MICOM, is an updated version of the Bergen Climate Model, BCM (Furevik et al., 2003; Otterå et al., 2009). The sea-ice model (CICE4) and the land model (CLM4) in NorESM are the same as in CCSM4.0,

ACPD
12, 18379–18418, 2012

except that the deposition of BC and mineral dust aerosols onto snow and sea-ice are given by CAM4-Oslo instead of using pre-calculated deposition fields which are used in CCSM4.0.

2.1.1 Aerosols in NorESM

The prognostic aerosols and aerosol precursors in CAM4-Oslo include sea-salt, mineral dust, DMS, SO_2, SO_4, BC and particulate OM and they interact online with the cloud microphysics, radiation and dynamics in the model. The present-day (2000) emissions are taken from Lamarque et al. (2010). Aerosol optical properties and size distributions (for calculation of cloud droplet number concentrations, CDNC) are calculated by use of look-up tables, where the entries in the tables are calculated by a single air parcel model for a wide range of atmospheric conditions. Both the direct effect and the first and second indirect effects are calculated. The direct effect of aerosols is caused by the scattering and absorption of radiation, mainly in the shortwave spectrum. The indirect effects of aerosols are due to their interaction with clouds, by acting as cloud condensation nuclei or ice nuclei. The aerosols can change the number and size of cloud droplets (the first indirect effect) and the lifetime of clouds (the second indirect effect). In the model the only process which causes the second indirect effect is the autoconversion of cloud droplets to precipitation in warm clouds (Storelvmo et al., 2008). Absorbing aerosols embedded in or near a cloud layer may also reduce the cloud cover by heating the air and promoting cloud evaporation, leading to a positive semi-direct effect (Hansen et al., 1997). In the look-up tables, size distributed aerosol number concentrations and composition, as well as bulk optical properties, have been calculated from basic physico-chemical processes. The concentrations are tagged according to size mode (nucleation, aitken, accumulation, coarse) and production mechanism (nucleation, condensation, coagulation, aqueous chemistry).

BC is emitted from open biomass burning (42 %), fossil fuel combustion (38 %) and biofuels (20 %). The total annual emissions of BC are 7.7 $\mathrm{Tg\,yr^{-1}}$. When emitted from biomass burning, BC and OM are assumed internally mixed with each other. Primary

ACPD
12, 18379–18418, 2012

BC particles are emitted as nucleation and accumulation mode BC and internally mixed aitken mode OM and BC. Externally mixed BC is hydrophobic, and turns gradually into hydrophilic, internally mixed aerosols by condensation of gaseous sulphate, or by coagulation with sulphate or SS or OM. BC is removed from the atmosphere by dry deposition and wet removal, although the latter process dominates the total numbers.

2.2 Experimental setup

The model is set up with a Finite Volume dynamical core with 26 vertical layers and with a 1.9 × 2.5 horizontal grid resolution. For each simulation the model is run 60 yr from a 140 yr spin-up with the same initial conditions and the same present-day emissions. In the two perturbed simulations the model is run with the same emissions as the control run, but the BC concentrations are multiplied by a factor of 10 in the Arctic (60° N–90° N; "the ARC experiment") and mid-latitudes (28° N–60° N; "the MID experiment"), respectively. In order to get a significant climate signal in the 60 yr simulations, the BC concentrations have been multiplied by 10. It is worth noting that the number is higher than in Shindell and Faluvegi (2009). To keep the relative distribution of the BC aerosols as similar as possible within each latitude band, the perturbations of the BC concentrations have been done in the radiation code. Note that only atmospheric BC has been perturbed in this study and the radiative forcing from BC deposition on snow and ice has been studied elsewhere, e.g. Flanner et al. (2007), and lie outside the scope of this study. A summary of the experimental set-up is shown in Table 1.

2.3 The Arctic energy budget

To understand the responses in the Arctic climate due to the BC perturbations we analyze the energy budget of the Arctic atmosphere in detail. The forcing and the temperature response in the Arctic may influence the meridional temperature gradient, which may dampen or strengthen the atmospheric heat transport into the Arctic. When studying Arctic climate change and local feedbacks, it is important to include the energy

ACPD
12, 18379–18418, 2012

transport because of the strong coupling between Arctic feedback mechanisms and the energy transport into the Arctic (Hwang et al., 2011). The northward heat transport (NHT) is defined as the net atmospheric flux of heat from lower latitudes into the Arctic region. Following Porter et al. (2005) and Kay et al. (2012) the NHT can be calculated by looking at the energy budget for an atmospheric column,

$$\frac{\delta E}{\delta t} = F_{TOA} + F_{SURF} + NHT \quad (1)$$

E is the atmospheric energy storage, F_{TOA} is the net energy budget at the top of the atmosphere and F_{SURF} is the net energy budget at the surface. F_{TOA} is defined as:

$$F_{TOA} = SW_{TOA} + LW_{TOA} \quad (2)$$

SW_{TOA} is the net incoming shortwave radiation and LW_{TOA} is the net outgoing long wave radiation. F_{SURF} is defined as:

$$F_{SURF} = SW_{SURF} + LW_{SURF} + LHFLX + SHFLX \quad (3)$$

SW_{SURF} is the net surface shortwave radiation, LW_{SURF} is the net surface long wave radiation, LHFLX is the latent heat flux and SHFLX is the sensible heat flux. The model is run with a fully coupled ocean model allowing for changes in the heat transport in the ocean. With the atmospheric perspective adopted here, the impact of this will be represented by a change in the surface fluxes.

We use the same sign convention as Porter et al. (2005), with all terms defined positive when the atmosphere gains energy; positive downward for the F_{TOA} and positive upward for the F_{SURF}. For annual averages, the energy storage term is small and negligible compared to F_{TOA}, F_{SURF} and NHT. The net atmospheric NHT can then be calculated as a residual of the remaining terms, F_{TOA} and F_{SURF}.

ACPD
12, 18379–18418, 2012

3 Simulated black carbon

3.1 BC concentrations

The simulated annual mean BC column burden, the zonal annual mean BC concentrations and the monthly mean BC column burden in the Arctic for the reference run with year 2000 emissions are shown in Fig. 1. Because of the short lifetime of BC on the order of days, the concentrations are largest close to the source regions near the surface; over densely populated and industrialized areas in China, Europe and the United States and over areas with biomass burning in Africa and South America. In the Arctic, on the other hand, the concentrations increase with height and the maximum concentrations are found in the middle troposphere. The strong static stability in the Arctic suppresses turbulent mixing between the surface and the upper troposphere, in particular during winter and early spring. The global mean BC column burden in the model is 0.28 mg m^{-2}. This is in good agreement with the multi-model mean value of 0.25 mg m^{-2} in the AeroCom model intercomparison project (Schulz et al., 2006). Averaged in each latitude band, the BC column burden is 0.19 mg m^{-2} in the Arctic and 0.36 mg m^{-2} in the mid-latitudes. In the model, the BC concentrations have a strong seasonal pattern in the Arctic, with a build up during winter, due to a combination of stronger northward transport and longer lifetime of the aerosols (Bauer et al., 2010; Liu et al., 2011; Lund and Berntsen, 2011). In the model this leads to a maximum in the BC column burden in the Arctic during May.

A comparison of the observed and modeled surface BC concentrations of three Arctic stations is included in Fig. 2. The measurements from Barrow are from the NOAA GMD database (www.esrl.noaa.gov/gmd) and measurements from Zeppelin station are provided by K. Eleftheriadis and S. Vratolis (Eleftheriadis et al., 2009) from the EBAS database (http://ebas.nilu.no). The measurements for the Alert station are provided by S. Sharma at Environment Canada. The measured concentrations peaks during the wintertime build-up of Arctic haze and have a summertime minimum. The model is able to simulate the seasonal cycle for Alert and Zeppelin, but the peak in the modeled

ACPD
12, 18379–18418, 2012

concentrations is later in the spring and the modeled surface concentrations are too low during winter. Generally, climate models tend to underestimate of wintertime surface BC concentrations in the Arctic compared to measurements (Shindell et al., 2008).

3.2 BC forcing in the Arctic and the mid-latitudes

The direct and indirect radiative forcing of BC is calculated as the difference in incoming and outgoing solar radiation at the TOA between the perturbed runs with 10·BC concentrations in the mid latitude band (MID) and the Arctic band (ARC) and the control run with 1·BC concentrations (2000 conditions). The radiative forcing is calculated in separate offline simulations with identical meteorology in 5 yr simulations for the 3 simulations. The meteorology is driven by NCAR CAM4 aerosols, prescribed CDNC and greenhouse gases. In the online 60 yr simulations the aerosol, cloud and radiation is fully coupled and thus the meteorology is different from the offline simulations. The annual 28° N–60° N mean direct radiative forcing at the TOA for 10·BC perturbed concentrations in the mid-latitudes is estimated to 7.3 $W m^{-2}$ (1.5 $W m^{-2}$ global average) and the indirect forcing is estimated to 0.20 $W m^{-2}$ (0.030 $W m^{-2}$). For 10 BC perturbed concentrations in the Arctic the estimated annual 60° N–90° N mean direct radiative forcing at the TOA is 6.0 $W m^{-2}$ (0.40 $W m^{-2}$) and the indirect local forcing at the TOA is 0.10 $W m^{-2}$ (0.010 $W m^{-2}$). The geographical distribution of the BC annual mean direct radiative forcing from ARC and MID is shown in Fig. 3. The distribution depends on the column burden of BC, but also on the albedo of the underlying surface, vertical distribution of the aerosols relative to the clouds and the amount of incoming solar radiation. The high surface albedo in the Arctic regions causes the BC radiative forcing to be large in this area, despite the smaller BC burden (see Fig. 1). The forcing effiency (RF normalized to burden change) is thus significantly higher in the Arctic (3600 $W g^{-1}$) than at mid-latitudes (and 2300 $W g^{-1}$). For comparison a global forcing efficiency for all present-day BC (compared to a run with zero BC) was calculated to 3100 $W g^{-1}$. In the fully coupled simulations there can be a small radiative forcing outside the region where the BC concentrations are scaled up (i.e. the ARC or the MID region), because

ACPD
12, 18379–18418, 2012

of the changes in surface and cloud albedo and redistribution of BC due to changes in circulation and scavenging rates. The indirect effect of BC aerosols is largest over the oceans, and is much smaller than the direct radiative effects of BC.

Figure 4 shows the monthly mean BC direct radiative forcing at TOA for the ARC experiment (60° N–90° N average) and the MID experiment (28° N–60° N average). The forcing peaks in May in the Arctic (15 W m^{-2}) for several reasons; the solar insolation and the BC concentrations are both close to their maxima, and it is early in the melt season, with still a great amount of snow and ice-covered surface with a high surface albedo. During the polar night, the Arctic forcing approaches zero. The mid latitude forcing peaks in the summer, but is still fairly high during the winter months, due to a combination of higher solar radiation in the mid-latitudes compared to the Arctic, as well as higher emissions and surface albedo in the mid-latitudes during winter compared to the summer season.

4 Climate response and feedbacks

The change in the vertical temperature profile for the ARC and the MID experiment is shown in Fig. 5. In both experiments the temperature increases above 800 hPa. The maximum temperature increase is found around 200 hPa, in the latitude band where the BC profile has been scaled up. The temperature increase is larger over a much larger volume of the atmosphere for the MID experiment than for the ARC experiment, in accordance with the larger global forcing for the MID experiment. In both our experiments the warming in the Arctic is most pronounced in the upper troposphere, but for very different reasons. In the ARC case warming is caused by the direct absorption of solar radiation by BC in the free troposphere, and further enhanced by semi-direct and surface albedo effects. In the MID experiment the heat is generated by absorption and heating at all altitudes at mid-latitudes, but since the transport to the Arctic mainly follows isentropic surfaces the maximum heating in the Arctic is also in this case in the upper troposphere. While there is a warming throughout the troposphere in the MID ex-

ACPD
12, 18379–18418, 2012

periment, the ARC forcing causes a cooling at the surface north of 60° N, in agreement with the response found by Shindell and Faluvegi (2009).

Figure 6 shows the seasonal cycle for the Arctic temperature response, averaged north of 60° N for both the ARC and the MID forcing. The cooling at the surface for the ARC forcing is prominent all year except in the summer months. In late summer and autumn the atmosphere is less stable and turbulence processes mix the heating in the atmosphere down to the surface. The warming of the Arctic surface in the summer is due to a combined effect of decreased static stability and increased downward longwave radiation and heat fluxes. In both experiments the warming increases rapidly with height, in particular during summer. The period of surface warming is not centered round mid summer in June when the incoming solar radiation is at its maximum, but is slightly skewed towards the autumn. In the autumn the snow/sea-ice cover in the Arctic is at its minimum, while in the spring and early summer the surface albedo is still high. For the MID forcing the surface warming is strongest during summer and autumn. The warming in the upper troposphere is strong during summer and continues until early autumn. It is worth noting that even in the MID case where there is no local forcing in the free troposphere due to enhanced absorption by BC, there is an equally strong vertical gradient in the warming and thus an increase in the static stability as in the ARC case.

The geographical distribution of the annual mean surface air temperature (SAT) response from the ARC and the MID forcing is shown in Fig. 7. The Arctic annual mean SAT response is −0.44 K for the ARC forcing with a cooling over most of the Arctic Sea and a warming over Greenland. There is a maximum cooling 2 K over the Barents Sea. For the MID forcing the Arctic annual mean SAT response is 1.07 K with a strong warming across the entire Arctic Ocean and with a maximum warming of 2 K over the Barents Sea. This area along the sea-ice edge is the area with the largest climate variability and large local feedbacks. Our results in general agree with the response in SAT from BC forcing in Shindell and Faluvegi (2009). Shindell and Faluvegi estimated an Arctic SAT response per unit global forcing of $-1.2\,\mathrm{K}\,(\mathrm{W\,m^{-2}})^{-1}$ from BC aerosols in the

ACPD
12, 18379–18418, 2012

Arctic and 0.8 K $(W m^{-2})^{-1}$ Arctic SAT response from BC aerosols in the mid latitudes. Our estimated Arctic SAT response per unit global forcing is −1.1 K $(W m^{-2})^{-1}$ from BC aerosols in the Arctic and 0.7 K $(W m^{-2})^{-1}$ from BC aerosols in the mid latitudes, respectively. The global SAT response per unit global forcing is 0.2 K $(W m^{-2})^{-1}$ for BC aerosols in the Arctic and in the mid latitudes, respectively, in accordance with Shindell and Faluvegi.

Shindell and Faluvegi explained the negative surface temperature response mainly as a result of a reduction in the pole-ward heat flux following local heating by absorbing BC aerosols. However, there are also significant changes in the surface energy fluxes due to direct and semi-direct effects of the BC aerosols as well as strong local feedbacks.

In the Arctic there is a net positive flux of sensible heat from the atmosphere to the surface. The increase in the static stability reduces the turbulent mixing that can transport the warm air in the free troposphere down to the surface.

By increasing the static stability, the BC aerosols have a positive semi-direct effect on the cloud cover in the Arctic. Both the ARC and the MID experiment show an increase in the Arctic cloud cover during summer when the cloud fraction is peaking (Fig. 8). The annual increase is largest in the MID experiment, while the change is about equal during the summer months. The increase in the cloud cover can also be linked to feedbacks to the surface temperatures response. The SAT response for both the ARC and the MID experiment are positive during the summer and there is a strong coupling between the surface and the atmosphere with increased upward fluxes of moisture and heat. When autumn starts, and the SAT response for the ARC experiment turns negative, the response in low cloud fraction falls to zero, while it stays positive for the MID experiment the whole year, following the positive SAT response. Kay and Gettelman (2009) found, using observations and atmospheric reanalysis, that near-surface static stability and surface cover can exert significant control on low Arctic cloud presence. It is worth noting that the Arctic clouds in the model are too optically thick because they have excessive liquid water paths when compared to observations (de Boer et al.,

ACPD
12, 18379–18418, 2012

2011; Kay et al., 2012). The geographical distribution of the annual mean cloud fraction is shown in Fig. 9. The cloud cover change is negative in the Barents Sea in the ARC experiment, following the increase in sea ice and cooling of the surface in this area. The cloud cover increases in most parts in the Arctic for the MID experiment, and also over oceans in the mid latitudes, while there is a decrease in cloud fraction over land in the mid-latitudes and along the east coast of Greenland. The BC concentrations over land areas in the mid-latitudes are highest close to the surface (see Fig. 1). Over the oceans, however, the BC aerosols are located higher up in the atmosphere and may enhance the underlying stratocumulus clouds, by stabilizing the atmosphere beneath, and reduce mixing with dry air above (Johnson et al., 2004).

The response in the surface temperatures is enhanced by sea-ice albedo feedbacks. The geographical distribution of the changes in the sea-ice concentrations are shown in Fig. 10. For the ARC forcing there is an increase in sea-ice concentration. The geographical pattern closely resembles the geographical patterns of the surface temperature response. For the MID forcing there is a corresponding decrease in the sea-ice following warmer surface temperatures. This response clearly depicts the Arctic amplification as the increase (decrease) in sea-ice triggers the colder (warmer) surface temperatures.

The changes in the sea-ice cover resemble the changes in the surface albedo, with an increase in the albedo for the ARC experiment where there is increased sea-ice cover and a decrease in the albedo for the MID experiment (Fig. 11). For both experiments the maximum change in the albedo is in October.

5 Heat budget analysis

Despite the positive BC forcing at TOA, the surface temperature response in the Arctic is negative for the ARC forcing, and positive for the MID forcing. In order to explain how BC aerosols affect the Arctic climate, we have analyzed the energy budget in the Arctic in detail. A summary of the change in the Arctic annual mean energy budget terms

ACPD
12, 18379–18418, 2012

for the two experiments is given Fig. 12. Note that all fluxes are defined positive when the atmosphere gains energy. For the ARC experiment, the primary forcing through the absorption of solar radiation by the BC aerosols gives a large increase in the net downward SW flux at the TOA. The associated warming of the air in the free troposphere leads to an increase in the outgoing LW flux at TOA (thus the negative change in Fig. 12). At the surface, there is a significant reduction in the downward SW flux due to the dimming effect of the absorption by the BC aerosols. Also the semi-direct effect of the BC aerosols and surface feedbacks lead to increased cloudiness and surface albedo that contribute to the reduction in the net downward SW flux at the surface in the ARC case. The reductions in the fluxes of latent and sensible heat are mainly a result of sea ice feedback in the Barents Sea. The reduction in the latitudinal temperature gradient in the free troposphere leads to a substantial reduction in the NHT (cf. discussion below). For the MID experiment the primary forcing is located outside the Arctic region, thus the change in the net SW flux at the TOA is small. However, the heating of the free troposphere by increased NHT and the increase in surface temperatures lead to an increase in the outgoing LW radiation at TOA which is larger than in the ARC case. The change in the net SW flux at the surface is much smaller in the MID case because there is no direct dimming effect and because the changed surface albedo and cloudiness counteract each other in this case.

Figure 13 shows the seasonal cycle of the Arctic mean energy budget at TOA, and at the surface and the residual NHT, for the reference control run (top) and for the corresponding changes in the ARC and MID experiments (bottom). In the reference simulation there is a net radiative loss at the TOA all year except in June and July, reflecting the peak in the incoming SW radiation and the melting of snow and ice that reduces the albedo. At the surface, the net flux to the atmosphere is positive during the winter season, when energy is transferred from the surface to the cold atmosphere, and negative during summer. The energy fluxes at the TOA and at the surface are in balance with the NHT, which has a maximum in the winter corresponding to about 120 $\mathrm{W\,m^{-2}}$ (4.1 PW at 60° N) and a minimum during summer at about 30 $\mathrm{W\,m^{-2}}$ (1.0 PW

ACPD
12, 18379–18418, 2012

at 60° N). The NHT is largest during winter when the meridional temperature gradient is at its maximum. For the ARC experiment the change in the NHT is negative, closely following the seasonal cycle in the primary forcing at the corresponding temperature signal. During winter when the BC forcing is small and the net change in the surface fluxes is negative due to sea-ice feedback, the change in the NHT is positive. The decrease in the NHT is likely to be a result of the increase in the temperatures in the upper Arctic troposphere, decreasing the meridional temperature gradient. The decrease is largest during the summer season, when the temperature increase in the upper troposphere is largest (Fig. 6). For the MID forcing, however, the change in the NHT is positive, consistent with the large positive temperature response in the mid-latitudes, increasing the meridional temperature gradient between the mid-latitudes and the Arctic, and increasing the heat transport into the Arctic.

Figure 14 shows the seasonal cycle of the changes in the Arctic mean SW and LW radiative fluxes at the TOA for the two perturbed experiments. The seasonal cycle in the TOA radiative imbalance (SW + LW, green curves) is very different in the two experiments. In the ARC case it is positive and follows the seasonal cycle in the primary forcing (SW) with a sharp peak in late spring (June), while in the MID case it is negative mainly through the changes in the LW fluxes governed by transport of heat and feedbacks, and with a much broader maximum during later summer and fall. The change in the Arctic mean SW flux is close to zero for the MID experiment. The outgoing LW radiation in the Arctic increases for both perturbed runs, consistent with a warmer free troposphere. The increase in the outgoing LW radiation is largest during the summer season for both runs, when the temperatures are peaking. For the MID forcing the increase in outgoing LW radiation is prominent all year. The outgoing LW is largest for the MID experiment due to the heating of the free troposphere by the increase in the NHT.

Figure 15 shows the seasonal cycle of the Arctic mean energy fluxes at the surface for the control run (top) and for the change in the fluxes between the control run and the two experiments (bottom). The net SW flux increases for both experiments, with

ACPD
12, 18379–18418, 2012

the largest increase in the ARC experiment. The increase in the net SW flux means that less radiation is reaching the surface, consistent with increased SW absorption by BC higher up in the atmosphere and increased cloudiness, and/or an increase in the amount of reflected radiation from the surface, due to the higher surface albedo (see Fig. 11). The decrease in downwelling solar radiation is twice as large for the ARC experiment as for the MID experiment ($5\,W\,m^{-2}$ vs. $2.6\,W\,m^{-2}$). Even though the surface albedo increases in the ARC experiment, the total amount of radiation reaching the surface is smaller, so the net change in the reflected SW flux is negative. The MID run shows a decrease in the net SW flux in the areas with decreased sea-ice, consistent with increased absorption of SW by the exposed darker ocean in a warmer climate, but also increases over large areas where there is an increase in cloudiness. Thus, averaged over the Arctic domain the change in SW flux in the MID experiment is positive.

The net (up–down) longwave flux at the surface decrease for both experiments, which means that more longwave radiation is transferred to the surface from the atmosphere. The factors causing this change are changes in the air temperature and cloudiness as well as the surface temperatures which again is mainly driven by changes in the sea ice cover. For the MID experiment there is increased net longwave flux at the sea-ice-edge where more long wave radiation is emitted to the atmosphere when the sea-ice melts.

In the reference run, the sensible heat flux is negative over the Arctic Ocean, associated with the temperature inversion caused by the net radiative energy loss from the surface. The Arctic mean change in the sensible heat flux is negative for both experiments, so more energy is transported from the atmosphere to the surface. However, the geographical distribution for the change in sensible heat flux differs for the two experiments. For the ARC experiment, the sensible heat flux decreases in the areas were the surface temperatures decreases and the sea-ice extent increases. For the MID experiment, the sensible heat flux increases over the Arctic Ocean, consistent with decreased sea-ice extent. The latent heat flux is reduced for the ARC experiment, consistent with

ACPD
12, 18379–18418, 2012

the colder surface temperatures, while the latent heat flux is slightly increased during autumn for the MID experiment. During the summer months, the longwave radiative flux and the heat fluxes for the ARC experiment have a minimum (more flux to the surface), resulting in a surface warming (see Fig. 6).

6 Summary and conclusion

BC aerosols heat the surrounding air and alter the local static stability and the vertical motions in the atmosphere. Regional changes in the BC concentration also change the temperature gradients affecting the meridional heat transport. Using the NorESM model we find that when BC concentrations are scaled up in the Arctic according to its current vertical profile, the surface temperature response is negative despite a positive radiative forcing at TOA. The Arctic surface temperature responses are similar to the results found in Shindell and Faluvegi (2009). We find that the BC climate response has a regional nature and this regionality results from surface albedo feedbacks. The surface cooling can be explained by a combination of changes in the vertical fluxes of heat and radiation and a reduction in the meridional heat transport from lower latitudes. There is an upper troposphere heating by absorption of SW radiation, a surface dimming effect that reduces the downwelling solar radiation leading to an increase the static stability in the Arctic that suppress the turbulent mixing of the heat to the surface and increases the cloud cover. The reduction in the meridional heat transport is caused by a reduction in the meridional temperature gradient consistent with the maximum entropy production principle (Kleidon, 2009). The decrease in surface temperatures leads to a negative snow/ice albedo feedback. Even though BC aerosols are mainly emitted in the mid- latitudes and only a small fraction enter the Arctic, they may impact the Arctic climate. We estimate that BC aerosols at mid-latitudes lead to increased transport of heat into the Arctic, causing a warming, both at the surface and in the whole atmospheric column. The largest increase in the temperatures is found in the upper troposphere during summer due to transport of heat along isentropic surfaces. In this case

ACPD
12, 18379–18418, 2012

the temperature response is enhanced through snow/ice albedo feedback. In a recent study, Allen et al. (2012) argued that BC and tropospheric ozone are the main drivers of the Northern Hemisphere expansion, by heating primarily in the mid latitudes, causing a poleward shift in the storms tracks. In our study we find that the increased local warming in the mid latitudes by the BC aerosols cause a poleward shift of the jet stream and a poleward displacement of the maximum meridional temperature gradient.

Our idealized model calculations indicate that atmospheric BC forcing outside the Arctic is more important for the Arctic climate change compared to the forcing in the Arctic itself. Although the albedo effect of BC on snow does show a more regional response to an Arctic forcing, these results suggest that mitigation strategies for the Arctic climate should also address BC sources in locations outside the Arctic even if they don't contribute much to BC in the Arctic.

The temperature response to the BC forcing is linked to the vertical distribution of the BC aerosols. In idealized climate simulations Ban-Weiss et al. (2011) showed that as the altitude of the BC increases, the surface temperature response decreases. In this study we have scaled up the background vertical profile of the BC aerosols in the model, were most of the Arctic BC aerosols are located in the free troposphere. If the emissions of BC aerosols in the Arctic are increased in the future, e.g. by increased shipping or oil production, the BC aerosols would be emitted directly into the Arctic planetary boundary layer (PBL) and a different temperature response might be evident. The BC aerosols in the PBL would have a stronger interaction with the surface, both by deposition of BC on snow and ice and by radiative and sensible heat fluxes down to the surface. In this kind of model study it would be important to include the effect of the deposition of BC on snow and sea-ice covered surfaces.

Acknowledgement. We thank the Aerosol groups at the National Oceanic and Atmospheric Administation (NOAA), Global Monitoring Division for providing measurement data from Barrow, Konstantinos Eleftheriadis and Sterios Vratolis at the Institute of Nuclear Technology and Radiation Protection for providing measurement data from Zeppelin and Sangeeta Sharma at Environmental Canada for providing measurement data from Alert. We acknowledge the EBAS (http://ebas.nilu.no/Default.aspx) and the NOAA ESRL (http://www.esrl.noaa.gov/gmd)

ACPD
12, 18379–18418, 2012

databases. This study was partly funded by the Research Council in Norway through the Earthclim project, the Norwegian research Council's Programme for supercomputing (NOTUR) through a grant for computing time, and the ACCESS project supported by the European Commission 7th Framework Programme. The CESM project is supported by the National Science Foundation and the Office of Science (BER) of the US Department of Energy. The National Center for Atmospheric Research is operated by the University Corporation for Atmospheric Research under sponsorship of the National Science Foundation.

References

Allen, R. J., Sherwood, S. C., Norris, J. R., and Zender, C. S.: Recent Northern Hemisphere tropical expansion primarily driven by black carbon and tropospheric ozone, Nature, 485, 350–354, 2012.

AMAP: The Impact of Black Carbon on Arctic Climate, by: Quinn, P. K., Stohl, A., Arneth, A., Berntsen T., Burkhart, J., F., Christensen, J., Flanner, M., Kupiainen, K., Lihavainen, H., Shepherd, M., Shevchenko, V., Skov, H., and Vestreng, V., Arctic Monitoring and Assessment Programme (AMAP), Oslo, 72 pp., 2011.

Ban-Weiss, G. A., Cao, L., Bala, G., and Caldeira, K.: Dependence of climate forcing and response on the altitude of black carbon aerosols, Clim. Dynam., 38, 1–15, 2011.

Barrie, L. A.: Arctic air pollution: an overview of current knowledge, Atmos. Environ., 20, 643–663, 1986.

Bauer, S. E., Menon, S., Koch, D., Bond, T. C., and Tsigaridis, K.: A global modeling study on carbonaceous aerosol microphysical characteristics and radiative effects, Atmos. Chem. Phys., 10, 7439–7456, doi:10.5194/acp-10-7439-2010, 2010.

Chung, S. H. and Seinfeld, J. H.: Climate response of direct radiative forcing of anthropogenic black carbon, J. Geophys. Res., 110, D11102, doi:10.1029/2004JD005441, 2005.

de Boer, G., Chapman, W., Kay, J., Medeiros, B., Shupe, M. D., Vavrus, S., and Walsh, J.: A characterization of the present-day Arctic atmosphere in CCSM4, J. Climate, 25, 2676–2695, 2011.

Eleftheriadis, K., Vratolis, S., and Nyeki, S.: Aerosol black carbon in the European Arctic: measurements at Zeppelin station, Ny-Ålesund, Svalbard from 1998–2007, Geophys. Res. Lett., 36, L02809, doi:10.1029/2008GL035741, 2009.

ACPD
12, 18379–18418, 2012

Flanner, M., Zender, C., Randerson, J., and Rasch, P.: Present-day climate forcing and response from black carbon in snow, J. Geophys. Res., 112, D11202, doi:10.1029/2006JD008003, 2007.
Furevik, T., Bentsen, M., Drange, H., Kindem, I., Kvamstø, N. G., and Sorteberg, A.: Description and evaluation of the Bergen climate model: ARPEGE coupled with MICOM, Clim. Dynam., 21, 27–51, 2003.
Gent, P. R., Danabasoglu, G., Donner, L. J., Holland, M. M., Hunke, E. C., Jayne, S. R., Lawrence, D. M., Neale, R. B., Rasch, P. J., Vertenstein, M., Worley P. H., Yang, Z.-L., and Zhang, M.: The community climate system model version 4, J. Climate, 24, 4973–4991, 2011.
Hansen, J. and Nazarenko, L.: Soot climate forcing via snow and ice albedos, P. Natl. Acad. Sci. USA, 101, 423–428, 2004.
Hansen, J., Sato, M., and Ruedy, R.: Radiative forcing and climate response, J. Geophys. Res., 102, 6831–6864, 1997.
Hansen, J., Sato, M., Ruedy, R., Lacis, A., and Oinas, V.: Global warming in the twenty-first century: an alternative scenario, P. Natl. Acad. Sci. USA, 97, 9875–9880, 2000.
Hwang, Y. T., Frierson, D. M. W., and Kay, J. E.: Coupling between Arctic feedbacks and changes in poleward energy transport, Geophys. Res. Lett., 38, L17704, doi:10.1029/2011GL048546, 2011.
IPCC: Climate change 2007: the physical science basis: contribution of Working Group I to the Fourth Assessment Report of the Intergovernmental Panel on Climate Change, Cambridge Univ. Press, Cambridge, UK and New York, NY, USA, 2007.
Iversen, T. and Seland, Ø.: A scheme for process-tagged SO_4 and BC aerosols in NCAR CCM3: validation and sensitivity to cloud processes, J. Geophys. Res., 107, 101029, doi:10.1029/2001JD000885, 2002.
Iversen, T. and Seland, Ø.: Correction to "A scheme for processtagged SO_4 and BC aerosols in NCAR-CCM3. Validation and sensitivity to cloud processes", J. Geophys. Res., 108, 101029, doi:10.1029/2003JD003840, 2003.
Jacobson, M. Z.: Short-term effects of controlling fossil-fuel soot, biofuel soot and gases, and methane on climate, Arctic ice, and air pollution health, J. Geophys. Res., 115, D14209, doi:10.1029/2009JD013795, 2010.
Johnson, B. T., Shine, K. P., and Forster, P. M.: The semi-direct aerosol effect: impact of absorbing aerosols on marine stratocumulus, Q. J. Roy. Meteor. Soc., 130, 1407–1422, 2004.

ACPD
12, 18379–18418, 2012

Kay, J. E. and Gettelman, A.: Cloud influence on and response to seasonal Arctic sea ice loss, J. Geophys. Res, 114, D18204, doi:10.1029/2009JD011773, 2009.
Kay, J. E., Hillman, B. R., Klein, S. A., Zhang, Y., Medeiros, B., Pincus, R., Gettelman, A., Eaton, B., Boyle, J., and Marchand, R.: Exposing global cloud biases in the community atmosphere model (CAM) using satellite observations and their corresponding instrument simulators, J. Climate, doi:10.1175/JCLI-D-11-00469.1, in press, 2012.
Kay, J. E., Holland, M. M., Bitz, C. M., Blanchard-Wrigglesworth, E., Gettelman, A., Conley, A., and Bailey, D.: The influence of local feedbacks and northward heat transport on the equilibrium Arctic climate response to increased greenhouse gas forcing in coupled climate models, J. Climate, doi:10.1175/JCLI-D-11-00622.1, in press, 2012.
Kirkevåg, A., Iversen, T., Seland, Ø., Debernard, J., Storelvmo, T., and Kristjánsson, J.: Aerosol-cloud-climate interactions in the climate model CAM-Oslo, Tellus, 60, 492–512, 2008.
Kirkevåg, A., Iversen, T., Seland, Ø., Hoose, C., Kristjánsson, J. E., Struthers, H., Ekman, A., Ghan, S., Griesfeller, J., Nilsson, D., and Schulz, M.: Aerosol-climate interactions in the Norwegian earth system model – NorESM, in preparation, 2012.
Kleidon, A.: Nonequilibrium thermodynamics and maximum entropy production in the Earth system, Naturwissenschaften, 96, 653–677, 2009.
Koch, D. and Del Genio, A. D.: Black carbon semi-direct effects on cloud cover: review and synthesis, Atmos. Chem. Phys., 10, 7685–7696, doi:10.5194/acp-10-7685-2010, 2010.
Kristjánsson, J.: Studies of the aerosol indirect effect from sulfate and black carbon aerosols, J. Geophys. Res., 107, 4246, doi:10.1029/2001JD000887, 2002.
Lamarque, J.-F., Bond, T. C., Eyring, V., Granier, C., Heil, A., Klimont, Z., Lee, D., Liousse, C., Mieville, A., Owen, B., Schultz, M. G., Shindell, D., Smith, S. J., Stehfest, E., Van Aardenne, J., Cooper, O. R., Kainuma, M., Mahowald, N., McConnell, J. R., Naik, V., Riahi, K., and van Vuuren, D. P.: Historical (1850–2000) gridded anthropogenic and biomass burning emissions of reactive gases and aerosols: methodology and application, Atmos. Chem. Phys., 10, 7017–7039, doi:10.5194/acp-10-7017-2010, 2010.
Law, K. S. and Stohl, A.: Arctic air pollution: origins and impacts, Science, 315, 1537–1540, 2007.
Levy, H. I., Schwarzkopf, M. D., Horowitz, L., Ramaswamy, V., and Findell, K.: Strong sensitivity of late 21st century climate to projected changes in short-lived air pollutants, J. Geophys. Res., 113, D06102, doi:10.1029/2007JD009176, 2008.

ACPD
12, 18379–18418, 2012

Liu, J., Fan, S., Horowitz, L. W., and Levy II, H.: Evaluation of factors controlling long-range transport of black carbon to the Arctic, J. Geophys. Res., 116, D04307, doi:10.1029/2010JD015145, 2011.
Lund, M. T. and Berntsen, T.: Parameterization of black carbon aging in the OsloCTM2 and implications for regional transport to the Arctic, Atmos. Chem. Phys. Discuss., 11, 32499–32534, doi:10.5194/acpd-11-32499-2011, 2011.
Menon, S., Hansen, J., Nazarenko, L., and Luo, Y.: Climate effects of black carbon aerosols in China and India, Science, 297, 2250–2253, 2002.
Otterå, O. H., Bentsen, M., Bethke, I., and Kvamstø, N. G.: Simulated pre-industrial climate in Bergen Climate Model (version 2): model description and large-scale circulation features, Geosci. Model Dev., 2, 197–212, doi:10.5194/gmd-2-197-2009, 2009.
Pueschel, R. F. and Kinne, S. A.: Physical and radiative properties of Arctic atmospheric aerosols, Sci. Total Environ., 160, 811–824, 1995.
Schulz, M., Textor, C., Kinne, S., Balkanski, Y., Bauer, S., Berntsen, T., Berglen, T., Boucher, O., Dentener, F., Guibert, S., Isaksen, I. S. A., Iversen, T., Koch, D., Kirkevåg, A., Liu, X., Montanaro, V., Myhre, G., Penner, J. E., Pitari, G., Reddy, S., Seland, Ø., Stier, P., and Takemura, T.: Radiative forcing by aerosols as derived from the AeroCom present-day and pre-industrial simulations, Atmos. Chem. Phys., 6, 5225–5246, doi:10.5194/acp-6-5225-2006, 2006.
Seland, Ø., Iversen, T., Kirkevåg, A., and Storelvmo, T.: Aerosol-climate interactions in the CAM-Oslo atmospheric GCM and investigation of associated basic shortcomings, Tellus A, 60, 459–491, 2008.
Sharma, S., Andrews, E., Barrie, L., Ogren, J., and Lavoue, D.: Variations and sources of the equivalent black carbon in the high Arctic revealed by long-term observations at Alert and Barrow: 1989–2003, J. Geophys. Res., 111, D14208, doi:10.1029/2005JD006581, 2006.
Shindell, D.: Local and remote contributions to Arctic warming, Geophys. Res. Lett., 34, L14704, doi:10.1029/2007GL030221, 2007.
Shindell, D. and Faluvegi, G.: Climate response to regional radiative forcing during the twentieth century, Nat. Geosci., 2, 294–300, 2009.
Shindell, D. T., Chin, M., Dentener, F., Doherty, R. M., Faluvegi, G., Fiore, A. M., Hess, P., Koch, D. M., MacKenzie, I. A., Sanderson, M. G., Schultz, M. G., Schulz, M., Stevenson, D. S., Teich, H., Textor, C., Wild, O., Bergmann, D. J., Bey, I., Bian, H., Cuvelier, C., Duncan, B. N., Folberth, G., Horowitz, L. W., Jonson, J., Kaminski, J. W., Marmer, E., Park, R., Pringle, K. J., Schroeder, S., Szopa, S., Takemura, T., Zeng, G., Keating, T. J., and Zuber, A.:

ACPD
12, 18379–18418, 2012

A multi-model assessment of pollution transport to the Arctic, Atmos. Chem. Phys., 8, 5353–5372, doi:10.5194/acp-8-5353-2008, 2008.

Shindell, D., Kuylenstierna, J. C. I., Vignati, E., van Dingenen, R., Amann, M., Klimont, Z., Anenberg, S. C., Muller, N., Janssens-Maenhout, G., and Raes, F.: Simultaneously mitigating near-term climate change and improving human health and food security, Science, 335, 183–189, 2012.

Storelvmo, T., Kristjánsson, J., Lohmann, U., Iversen, T., Kirkevåg, A., and Seland, Ø.: Modeling of the Wegener-Bergeron-Findeisen process – implications for aerosol indirect effects, Environ. Res. Lett., 3, 045001, doi:10.1088/1748-9326/5/1/019801, 2008.

ACPD

12, 18379–18418, 2012

Table 1. Experimental setup for the CONTROL, ARC and MID experiments. PD = Present day emissions and levels of aerosols and green house gases. Local RF_{TOA} = the radiative forcing (both direct and indirect) at TOA averaged 60° N–90° N for the ARC-CONTROL experiment and averaged 28° N–60° N for the MID-CONTROL experiment. Units RF in $W m^{-2}$.

Experiment	Init. cond.	BC level in the atmosphere	Local RF_{TOA}	Global RF_{TOA}
CONTROL	PD	PD	–	–
ARC	PD	PD, 10·BC levels 60° N–90° N	6.1	0.41
MID	PD	PD, 10·BC levels 28° N–60° N	7.5	1.53

ACPD
12, 18379–18418, 2012

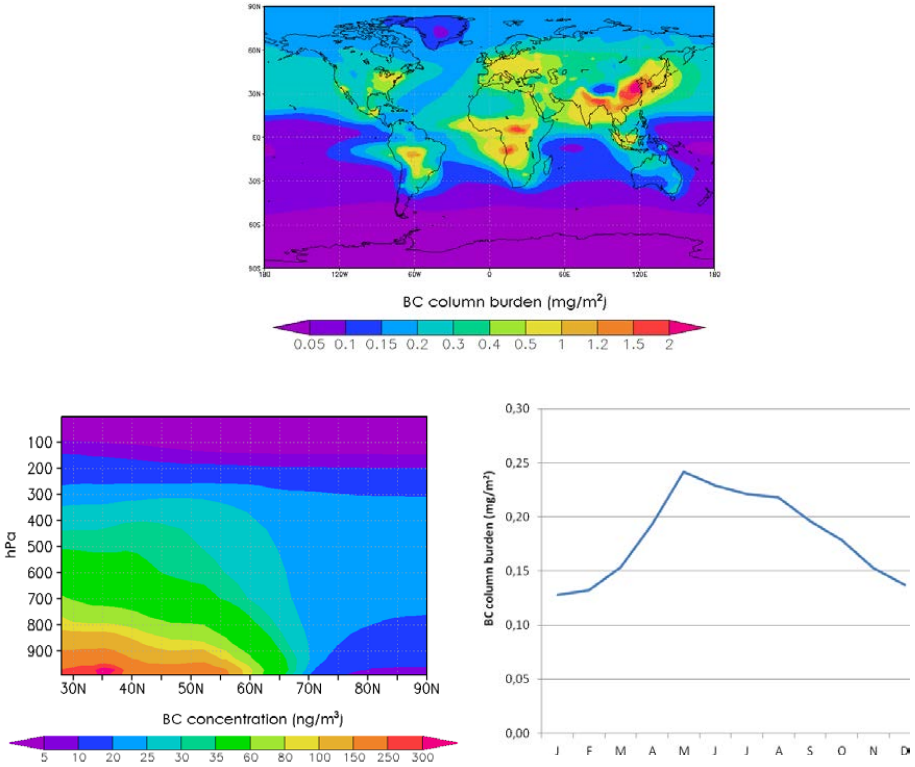

Fig. 1. Annual mean BC column burden (in mg m^{-2}) (top); zonal annual mean BC concentration (in µg m^{-3}) 28° N–90° N (bottom left) and monthly mean BC column burden (in mg m^{-2}) in the Arctic (bottom right) for the CONTROL run with 2000 emissions.

ACPD
12, 18379–18418, 2012

The Arctic response to remote and local forcing of black carbon

M. Sand et al.

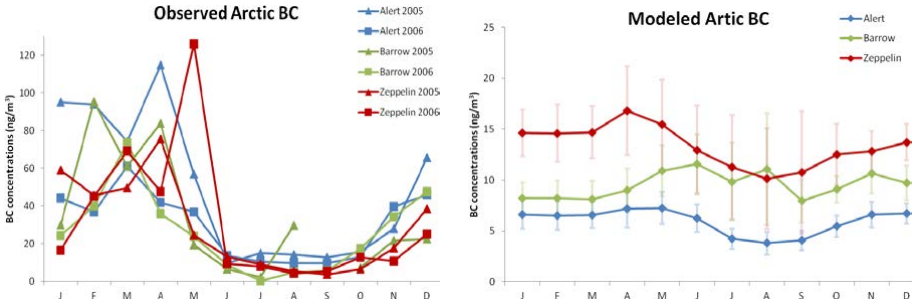

Fig. 2. Observed and modeled monthly mean BC concentrations from 3 Arctic stations (in ng m^{-3}). Note the different axes. The observed concentrations are from 2005 and 2006. The modeled concentrations are from the control run with one standard deviation shown as bars.

ACPD
12, 18379–18418, 2012

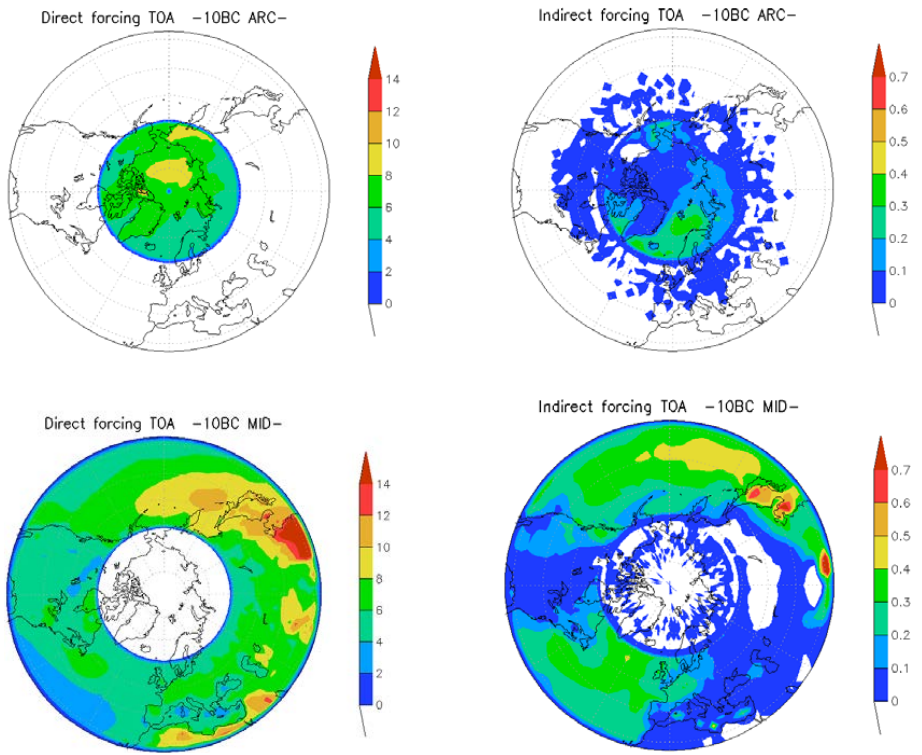

Fig. 3. Annual mean direct forcing (left) and indirect forcing (right) at the TOA (in $W m^{-2}$) for the ARC-CONTROL run (top) and the MID-CONTROL run (bottom).

ACPD
12, 18379–18418, 2012

The Arctic response to remote and local forcing of black carbon

M. Sand et al.

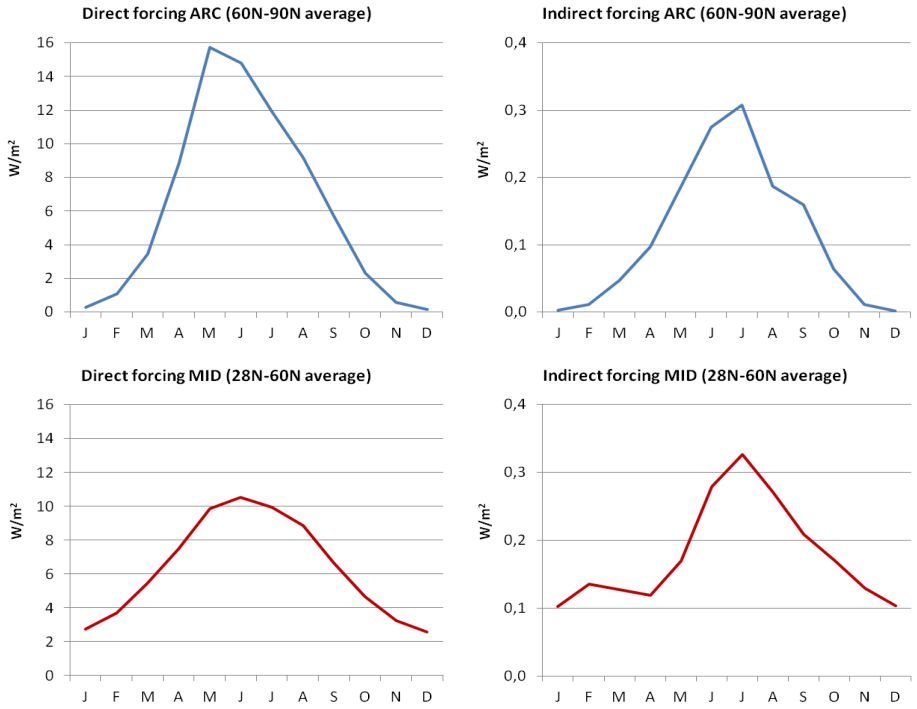

Fig. 4. Monthly mean direct forcing (left) and indirect forcing (right) (in $W m^{-2}$) at the TOA for the ARC-CONTROL run 60° N–90° N average (top) and the MID-CONTROL run 28° N–60° N average (bottom).

ACPD
12, 18379–18418, 2012

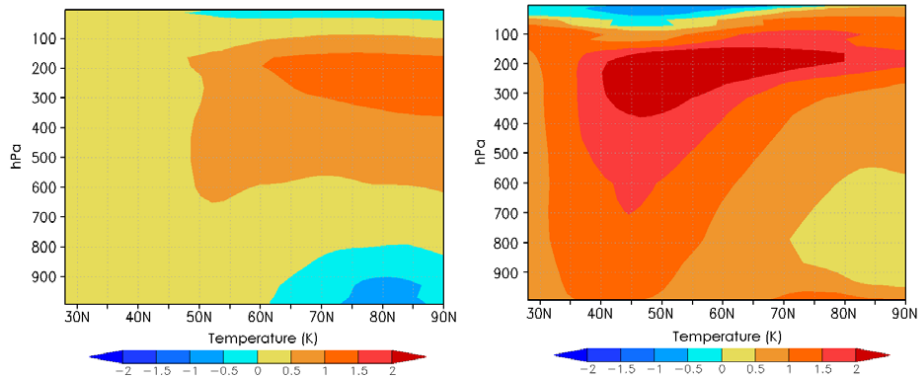

Fig. 5. Zonal annual mean temperature change (in K) for the ARC-CONTROL run (left) and the MID-CONTROL run (right).

ACPD
12, 18379–18418, 2012

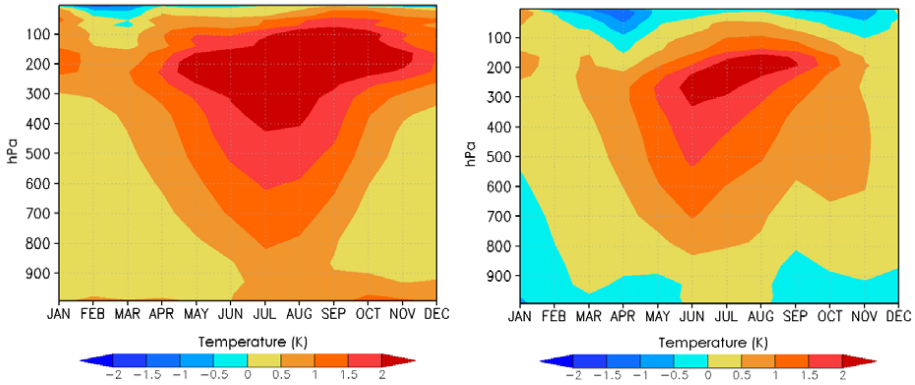

Fig. 6. Seasonal Arctic mean (60°N–90°N) temperature response (in K) for the ARC-CONTROL run (left) and the MID-CONTROL run (right).

ACPD
12, 18379–18418, 2012

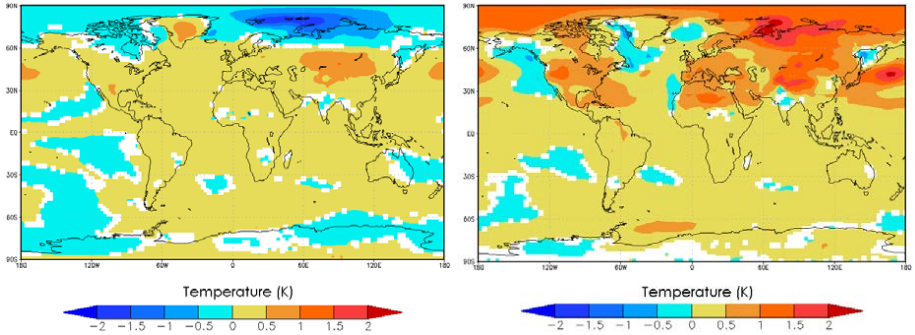

Fig. 7. Annual mean surface air temperature change (in K) for the ARC-CONTROL run (left) and the MID-CONTROL run (right). White areas are not significant on a 95 % level.

ACPD
12, 18379–18418, 2012

The Arctic response to remote and local forcing of black carbon

M. Sand et al.

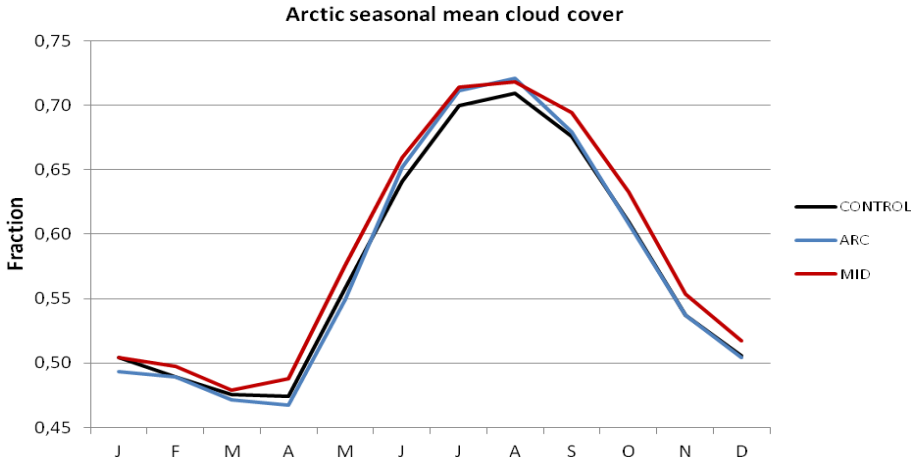

Fig. 8. Monthly Arctic mean cloud cover (in fraction) for the CONTROL run (black), the ARC experiment (blue) and the MID experiment (red).

ACPD
12, 18379–18418, 2012

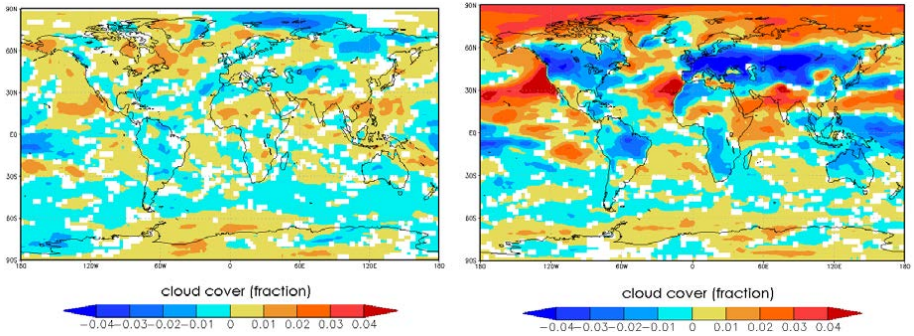

Fig. 9. ANN mean cloud cover change (in fraction) for the ARC-CONTROL (left) and the MID-CONTROL (right). White areas are not significant on a 95 % level.

ACPD
12, 18379–18418, 2012

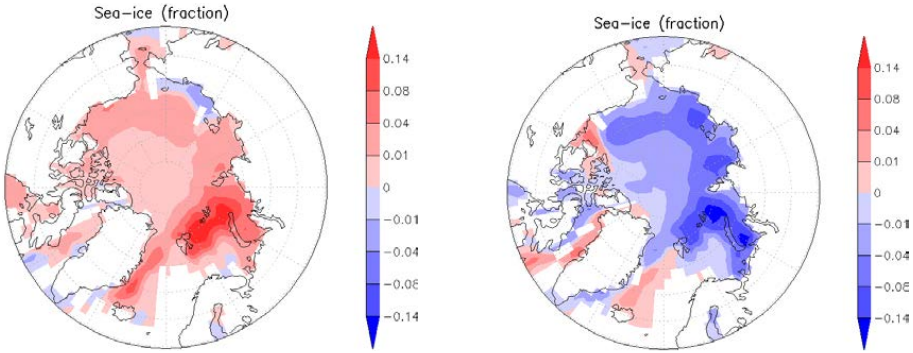

Fig. 10. Annual mean sea-ice cover change (in fraction) for the ARC-CONTROL (left) and the MID-CONTROL forcing (right). White areas are not significant on a 95 % level.

ACPD
12, 18379–18418, 2012

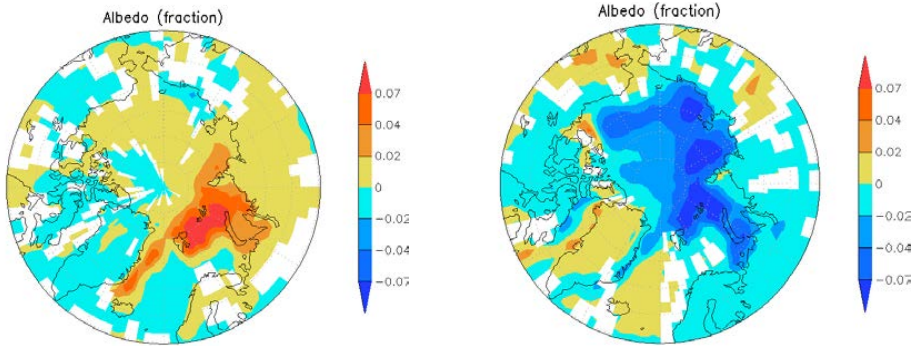

Fig. 11. Annual mean surface albedo response (in fraction) for ARC-CONTROL (left) and MID-CONTROL (right). White areas are not significant on a 95 % level.

ACPD
12, 18379–18418, 2012

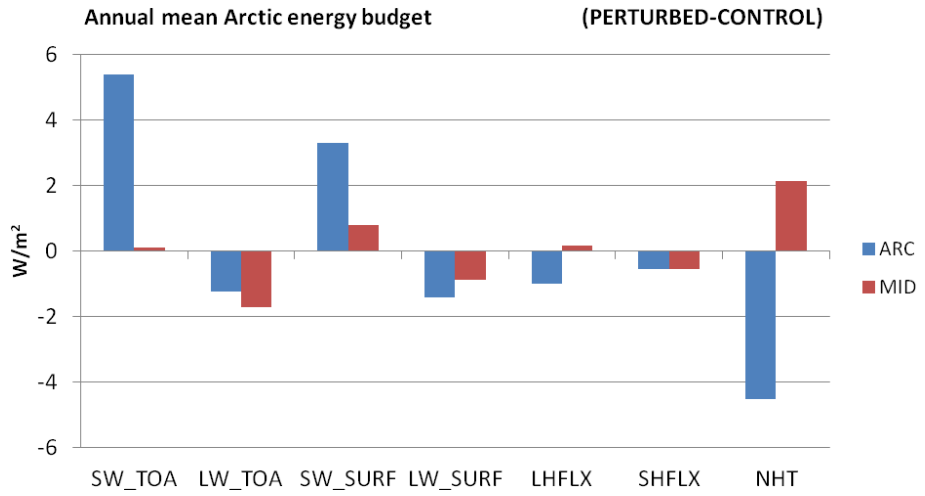

Fig. 12. Difference in the ANN Arctic mean energy budget terms for the ARC-CONTROL (blue) and MID-CONTROL (red). All units in $W m^{-2}$. SW_{TOA} and LW_{TOA} are the net SW and LW radiation fluxes at TOA; SW_{SURF} and LW_{SURF} are the net SW and LW radiation fluxes at the surface; LHFLX and SHFLX are the latent and sensible heat fluxes and NHT is the net atmospheric heat transport. All terms are defined positive when the atmosphere gains energy.

ACPD
12, 18379–18418, 2012

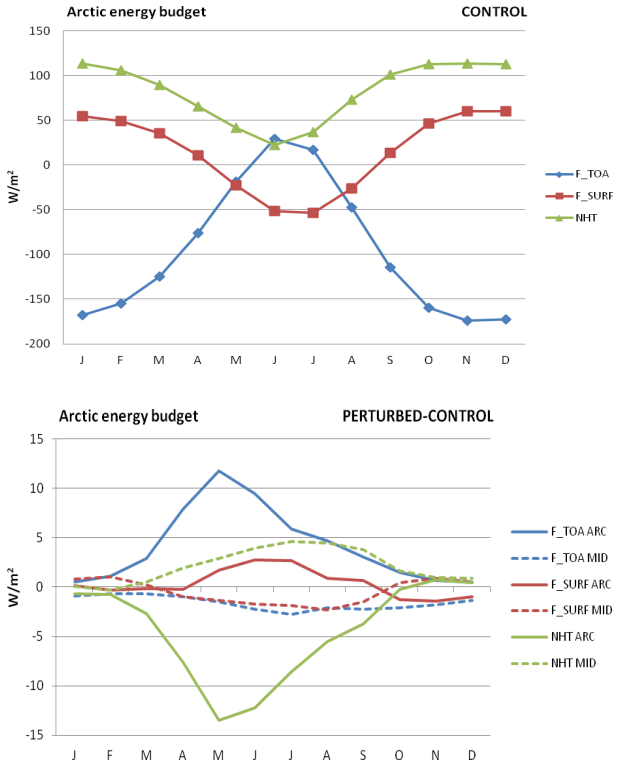

Fig. 13. Seasonal cycle of the Arctic energy budget terms for the Control run (top); net energy budget at TOA (blue), net energy budget at the surface (red) and the net atmospheric heat transport (green) and the corresponding changes (bottom); ARC-CONTROL (solid) and MID-CONTROL (dashed). All units in $W m^{-2}$. All terms are defined positive when the atmosphere gains energy.

ACPD
12, 18379–18418, 2012

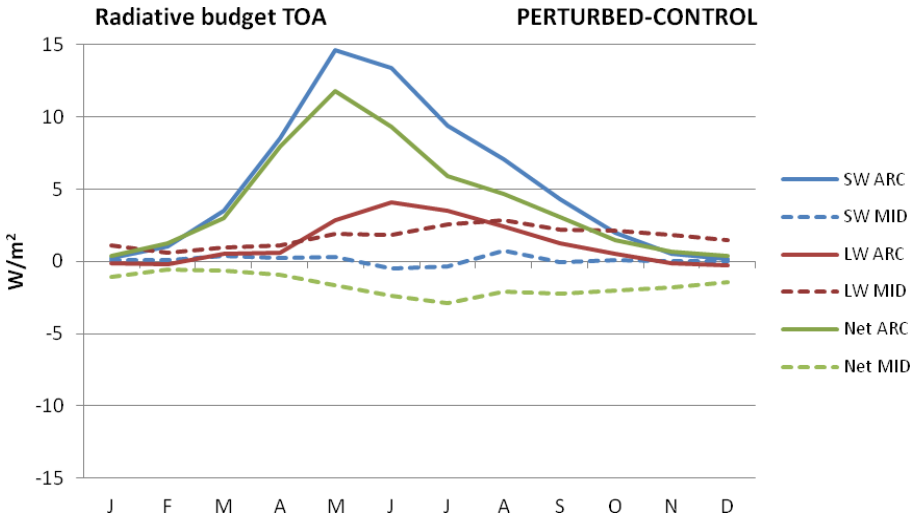

Fig. 14. Changes in the Arctic monthly mean radiative fluxes TOA; incoming SW (blue), outgoing LW (red) and net (green) for the ARC-CONTROL (solid) and MID-CONTROL (dashed). All units in $W m^{-2}$. All terms are defined positive when the atmosphere gains energy.

ACPD
12, 18379–18418, 2012

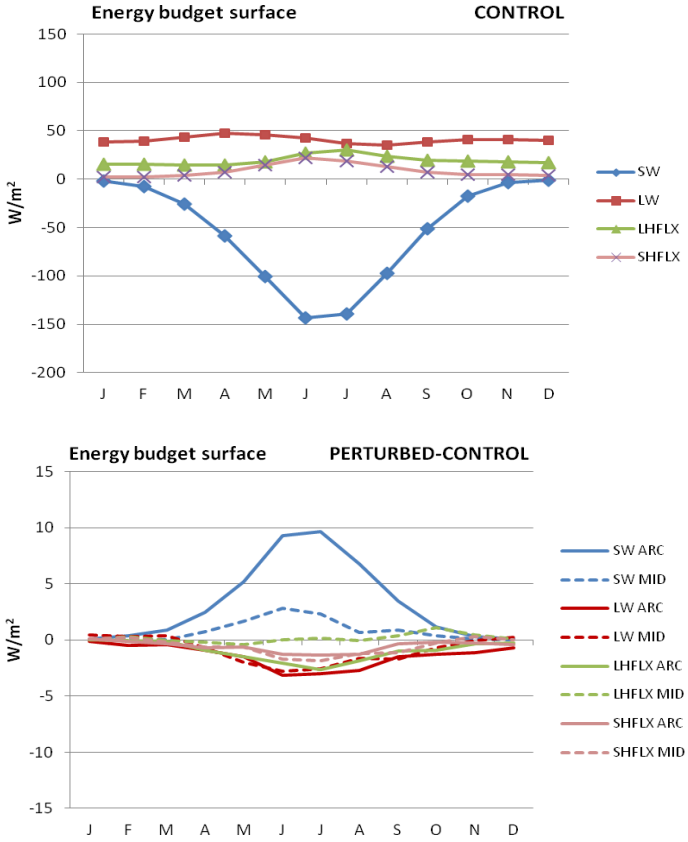

Fig. 15. Seasonal cycle of the Arctic mean energy fluxes at the surface for the CONTROL run (top); net SW radiation (blue); net LW radiation (red); latent heat flux (green) and sensible heat flux (pink), and the changes in the radiative fluxes ARC-CONTROL (solid) and MID-CONTROL (dashed) (bottom). All units in $W m^{-2}$. All terms are defined positive when the atmosphere gains energy.

ACPD
12, 18379–18418, 2012